Comparing Simulation Results from CHARM and RotCFD to the Multirotor Test Bed Experimental Data

Sarah Conley[1] and Dorsa Shirazi[2]

NASA Ames Research Center, Moffett Field, CA, 94035

ABSTRACT

Advanced multirotor vertical flight aircraft concepts are emerging faster than rigorous individualized tests can investigate their utility and performance. There are several analysis tools that predict multirotor performance and flow characteristics, but the accuracy of these predictions is still being debated due to lack of experimental data from multirotor tests that are needed to validate the analyses. The objective of this paper is to simulate multirotor configurations using two different mid-fidelity rotorcraft analysis tools, Comprehensive Hierarchical Aeromechanics Rotorcraft Model (CHARM) and Rotorcraft Computational Fluid Dynamics (RotCFD), and compare the simulation results to experimental data from a wind tunnel test of the Multirotor Test Bed (MTB). The MTB, developed by NASA Ames Research Center, is a new capability for testing a wide array of advanced vertical take-off and landing (VTOL) rotor configurations, with a primary focus on testing in the U.S. Army 7- by 10-Foot Wind Tunnel at NASA Ames Research Center. The MTB was designed to allow adjustment of the vertical, lateral, and longitudinal placement of up to six rotors, as well as allow tilt adjustment of each rotor and pitch adjustment of the whole assembly. The six-axis load cells under each rotor give the MTB the capability of measuring the rotor performance in a wide array of configurations. The overall goal of the MTB project is to help gain a better understanding of the performance, control, interactional aerodynamics, and acoustics of multirotor and tilting-rotor systems. For the work presented here, the MTB data were used to validate RotCFD and CHARM results for several multirotor test configurations. With confidence in both analyses established by the validation exercise, additional simulations were performed to explore quadrotor configurations that will be tested during the MTB's second wind tunnel entry planned for 2022. This second tunnel entry will examine quadrotor configurations that represent published NASA reference designs for urban air mobility concept vehicles. Results from this paper confirm the ability of RotCFD and CHARM to simulate multirotor aerodynamic interactions on individual rotor performance under edgewise forward-flight conditions.

NOMENCLATURE

ADM	= actuator-disk model	eVTOL	= electric vertical take-off and landing
CFD	= computational fluid dynamics	FF	= forward flight
CT	= thrust coefficient	FOM	= figure of merit
CP	= power coefficient	IDE	= integrated design environment
CVC	= constant vorticity contour	k	= turbulent kinetic energy
		MTB	= Multirotor Test Bed

[1] Mechanical and Aerospace Engineer, Aeromechanics Office, sarah.a.conley@nasa.gov

[2] Mechanical and Aerospace Engineer, Aeromechanics Office, dorsa.shirazi@nasa.gov

MUAS = multirotor unmanned aerial system

R = rotor radius

RPM = revolutions per minute

RVLT = revolutionary vertical lift technology

TE = tunnel entry

TnoB = tunnel no body

TwithB = tunnel with body

UAM = urban air mobility

UAS = unmanned aerial system

ε = rate of dissipation of k

σ = rotor solidity

1. INTRODUCTION

1.1 Background

Rotorcraft operate in a challenging environment of complex aerodynamics that are difficult to accurately simulate with Computational Fluid Dynamics (CFD) tools. Wind tunnel testing serves a critical role in providing validation data to help improve rotor performance predictions. Wind tunnel test data for multirotor systems have only recently started to become available, with the latest being from the Multirotor Test Bed in Fall of 2019. Two previous NASA wind tunnel tests of multirotor Unmanned Aerial System (UAS) vehicles were conducted in October – December 2015 [Ref.1] and January – February 2017 [Ref.2], [Ref.3], referred to as the MUAS1 and MUAS2 tests, respectively.

1.2 Multirotor Test Bed

The Multirotor Test Bed (MTB) project was initiated to build upon the knowledge and capabilities developed during the MUAS tests. By measuring individual rotor loads for a multirotor system and allowing for adjustments to individual rotor position and attitude, the MTB provides a wealth of data on the aeroperformance of arbitrary multirotor configurations. The flexibility in positioning up to 6 rotors on the MTB allows the multirotor design space to be parametrically explored and potentially optimized. The MTB is also at a larger scale than the small UAS tested before, which allows for testing at rotor tip Reynolds numbers more relevant to full-scale piloted electric vertical take-off and landing (eVTOL) aircraft. The MTB was tested in the U.S. Army 7- by 10- Foot Wind Tunnel in the Fall of 2019, see Figure 1.1. The experimental data from this first wind tunnel test, as noted earlier, will be discussed in this paper in the context of correlation and validation with the RotCFD and CHARM analysis tools, as applied to multirotor configurations in hover and edgewise forward flight.

Each rotor can tilt forward 90 deg and backwards 5 deg. In addition, the entire MTB can tilt forward 20 deg and backwards 10 deg. This flexibility allows the aggregate rotor system to be tested in many different multirotor and tilting-rotor configurations. A six-axis load cell under each rotor assembly measures both the steady and dynamic loads produced by each rotor. The wind tunnel scales can measure aerodynamic loads of the full assembly. For more information on the specific test capabilities of the MTB see [Ref.4]. Details of the MTB design are discussed in [Ref.5].

Many rotorcraft concepts with six (or more) rotors have been proposed by a number of different eVTOL companies (eVTOL being vehicles with some aspect of electric propulsion, capable of vertical takeoff and landing, as responding to potential Urban Air Mobility markets). To ultimately realize such vehicles and markets, significant wind tunnel and flight testing is still required to evaluate key design and operational parameters including performance, safety, and comfort for human passengers. In addition to allowing for the evaluation of the fundamental aerodynamics of rotor-on-rotor wake interactions, the test capabilities of the MTB are available for future tests of new multirotor aircraft concepts or rotor configurations. Such capability will aid in risk-reduction activities for organizations developing advanced eVTOL aircraft before committing to the expense and complexity of moving on to full-scale testing.

In this paper, results from several simulations using RotCFD and CHARM will be presented. The main objective of this paper is to compare the RotCFD and CHARM results with the experimental data from the MTB's first wind tunnel test and explore each analysis tool. The secondary objective is to use RotCFD and CHARM to simulate planned MTB configurations, for the upcoming second wind tunnel test, that might yield the best rotor performance, which could help determine which configurations should be explored in future wind tunnel tests. Additionally, this research can help quantify the effect of the wind tunnel walls and the MTB body on the performance of each rotor for a variety of MTB configurations.

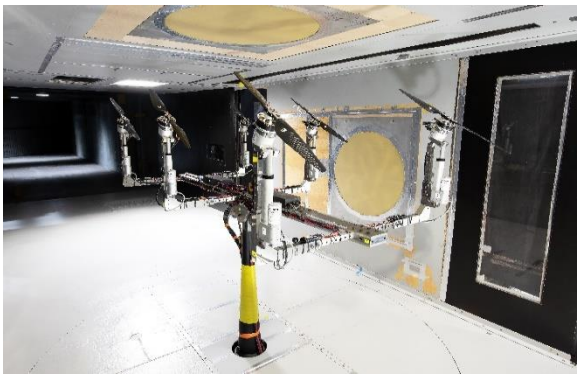

Figure 1.1 MTB in the U.S. Army's 7-by 10-Foot Wind Tunnel at NASA Ames Research Center.

1.3 RotCFD

One of the design tools used for this analysis is a mid-fidelity computational fluid dynamics (CFD) code RotCFD (Rotorcraft CFD), developed by Sukra Helitek, Inc. RotCFD uses an Integrated Design Environment (IDE) specific to rotorcraft, bridging the worlds of design and CFD [Ref.6][Ref.7]. The key components of RotCFD are a geometry module, a semi-automated grid generation module, a flow-solver module, a rotor module, and a flow visualization and analysis module, all integrated in one environment [Ref.7][Ref.8]. These modules allow rotorcraft performance metrics and flowfields to be simulated over time and analyzed in a Graphical User Interface (GUI).

The rotor blades are modeled using a blade element method (BEM) and are represented through the momentum they impart on the flow. Normally in CFD applications, a fully viscous, unsteady, body-conforming grid is used to compute the flow induced by the rotor, but representing the rotors by momentum sources from the BEM greatly reduces the computational time and complexity. The Reynolds-Averaged Navier-Stokes (RANS) equations provide the flowfield near the rotors using the rotor induced momentum sources and the blade element theory provides the forces on the rotor blades from the local velocity vector field. These equations are coupled implicitly to yield a self-contained method for generating unsteady performance, as well as the near and far wake including all the aerodynamic interferences present [Ref.7]. The reduced complexity of the simulations allows for complex flowfields to be analyzed on a single workstation with good results [Ref.9].

The rotor solution model used in RotCFD for this analysis is the actuator-disk model (ADM). A discrete-blade model is also available, but that model is more computationally expensive. The actuator-disk solution implicitly couples the external flowfield to the rotor via integrated momentum sources, whereas the discrete-blade solution couples the external flow to individual lifting lines, one for each blade. Both models require external airfoil tables so the program can calculate each blade section's lift, drag, and pitching moment. These sectional forces and moments are then converted to source terms, which are resolved along the blade span (using BEM) and averaged over the azimuthal locations (using ADM). This analysis uses the Rotorcraft Unstructured Solver (RotUNS) module which uses three-dimensional, unsteady Reynolds Averaged Navier-Stokes equations (URANS) on a Cartesian unstructured grid with tetrahedral body-fitting near the body [Ref.9]. The Semi-Implicit Method for Pressure-Linked Equations Revised (SIMPLER) is a line of pressure based algorithms which are used with the under-relaxation factors to iteratively compute the flowfield. Turbulence is accounted for by the URANS equations combined with a two-equation realizable $k-\varepsilon$ turbulence model with special wall treatment [Ref.9].

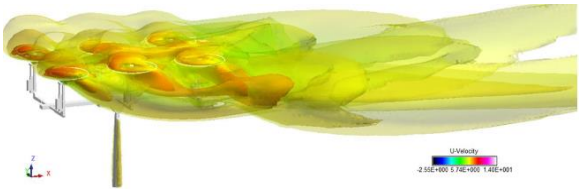

Figure 1.2 Flow visualization (showing U-velocity in m/s) of RotCFD simulation for 6-rotor case, tall rotor configuration, 20 ft/s tunnel speed, 0 deg pitch angle, with the MTB body in the tunnel, [Ref.11].

The internal grid generator, UGen, generates a Cartesian octree grid, starting from the domain boundary and then intersecting the body. The cells that intersect the geometry and the surrounding cells are sub-divided into tetrahedra, resulting in a grid that approximately conforms to the surface of the body. RotCFD accepts inputs on the specific rotor geometry, rotor RPM, tunnel speed, and tunnel conditions, used in the MTB wind tunnel tests. RotCFD then outputs the flow solution and individual rotor performance. Because RotUNS is unsteady, the flow changes with time can be observed. This study is seeking to not only validate this tool, but also validate the methods by which this tool is implemented (i.e. the airfoil table generation, talked about in section 2.1).

1.4 CHARM

CHARM is a comprehensive vertical take-off and landing (VTOL) aircraft tool developed by Continuum Dynamics Inc (CDI). CHARM is capable of modeling the VTOL aircraft aerodynamics in maneuvering and steady flight conditions. CHARM allows the user to define flow and body characteristics, including the rotor geometry, aerodynamic condition, wind tunnel speed, and airfoil tables as inputs. CHARM models the aircraft aerodynamic and dynamic interaction by combining the fast vortex and fast panel solution [Ref.13]. CHARM simulates real-time, free-wake instability in addition to computing performance of multiple rotors and interaction between the body and rotor wake. CHARM uses Constant Vorticity Contour (CVC) to model wakes [Ref.13][Ref.14] while providing accurate aerodynamic interaction results in a short computational time.

CHARM software uses the combination of fast vortex and fast panel solution methods to model the aircraft aerodynamic and dynamic interaction to deliver information such as load, trim, wake geometry, and surface pressure [Ref.12]. In the fast panel method, each panel has a constant source and doublet strength, where the source strengths satisfy the Dirichlet boundary conditions for the ambient flow filed. The Fast Vortex and Fast Panel method uses a grouping plan in addition to a validated multi-pole approximation to decrease the computational time by over two orders of magnitude for 10^5 panels. In the grouping technique, the vertices and panels are grouped into nested cells. For the high-density area, these grids will be more refined for nested cells. The solution is calculated through multipole expansion and Taylor series extrapolations.

Figure 1.3 Flow visualization of CHARM simulation (showing vorticity) of six rotors in short rotor configuration, 0 degree pitch, and 20 ft/s tunnel speed.

Moreover, CHARM uses the potential flow/panel method, which results in less CPU and memory compared to using RotCFD or even higher fidelity CFD like OVERFLOW. The potential flow/panel method is used to characterize the rotor wash from the presence of a wind tunnel or the fuselage's influence. The CVC improves wake geometry and induced velocity prediction. The CVC was also used to determine the swirl velocity profile and rolled up wakes.

2. METHOD

2.1 Airfoil Tables

The rotor selected for the MTB project was a two-bladed KDE-CF245-DP 2 made of carbon fiber – see Table 2.1. The rotor manufacturer data can be found at https://www.kdedirect.com/. The KDE rotor has a radius of 1.02 ft; this size was chosen to minimize the wall effect on the experimental data. A KDE rotor blade was laser-scanned, and the geometry of 25 airfoil sections was measured to define the blade spanwise geometry distribution. Note that the KDE rotor's tip was so thin that no airfoil shape could be resolved, and the rotor tip geometry was approximated. Four airfoil stations from the original 25, were selected at radial stations of r/R = 0.1891, 0.2662, 0.7515, and 0.9435 based on their maximum thickness, thickness position, leading edge radius, maximum camber, and maximum camber positions. The characteristics of the four primary airfoils should accurately capture any spanwise variation in these parameters when using a limited number of airfoils for the rotor model. Similar modeling strategies and airfoil table generation have been done in 2017 for CAMRAD II studies of small-scale UAS rotors, [Ref.21].

Table 2.1 The KDE rotor parameters.

Parameter	Value
Number of blades	2
Radius of blade	1.02 ft
Rotor disk area	3.27 ft^2
Rotor speed	2000 RPM

A table of lift coefficient, drag coefficient, and moment coefficient as a function of Mach number and angle-of-attack was generated for each of the four airfoil stations using XFOIL software [Ref.11, Kallstrom] [Ref.18]. These airfoil tables were generated by considering the environment and conditions such as wind tunnel speed, rotor speed, angle of attack, and Mach number that these four airfoil sections would experience. Since the local velocity is different at each airfoil station, the Reynolds number varies along the rotor span. Also,

each airfoil station experiences a different Reynolds number depending on the azimuth angle of the blade.

Table 2.2 shows airfoil stations, Reynolds numbers, and Mach numbers used in XFOIL to create the airfoil tables for the KDE rotor [Ref.18] [Ref.11, Kallstrom]. The airfoil tables in the look-up tables used for the simulations need to cover the full range of Mach numbers of any blade section that might occur during the simulation calculation. The KDE rotor airfoil tables were generated for the highest wind tunnel speed of 40 ft/s. The maximum Mach number for the advancing blade at each respective radial station was used as input to XFOIL for the airfoil table generation.

Table 2.2 Reynolds number of four main airfoil stations used to generate the airfoil tables in XFOIL.

r/R	Local Mach#	Local Re#
0.1891	0.03	18,543
0.2662	0.05	55,807
0.7515	0.14	127,780
0.9432	0.18	98,346

2.2 Simulation Test Matrices

2.2.1 Simulation test matrix of the 1st MTB TE

The MTB has been tested in the wind tunnel in numerous configurations during the first wind tunnel entry in 2019; for a full test matrix see [Ref.4]. The simulation test matrix was determined by choosing wind tunnel runs in which only one independent variable changed for each run, and therefore the effects of each variable could be easily observed. The target rotor speed for all cases was set to 2000 RPM, and the simulation test matrix is provided in Table 2.3. Three different types of cases were simulated in this study: TwithB, TnoB, and FF. The TwithB cases – "Tunnel with Body" – have the rotors and body of the MTB in a simulated tunnel (boundary of the simulation is the dimension of the tunnel walls). The TnoB cases – "Tunnel no Body" – have a simulated tunnel without the body of the MTB. Comparing results between the TwithB and the TnoB cases highlights the effects of the body on the flow and rotor performance. The FF cases – "Free Field" – significantly extend the computational boundary (or rather the planes of the computational domain on which the boundary conditions are applied) to reduce wall effects on the flow near the MTB. Essentially, the FF cases are rotors floating in mid-air with no body. The simulation excludes the body of the MTB. Comparing the results of the FF and the TnoB cases highlights the effects of the tunnel on the flow and rotor performance. For more details on the three case types see Reference 11.

The wind tunnel speed, static pressure, static temperature, static density, dynamic viscosity in the wind tunnel, and individual rotor RPM were recorded/calculated for each data point. These values were then used in the simulations of the different cases. The pitch angle of the MTB was assumed to be exactly -10, -5, or 0 deg for the different cases. The measured tunnel conditions for each case were used in the simulations to minimize potential sources of inaccuracy in the simulations. The six-axis load cells underneath each rotor provided the forces (Fx, Fy, and Fz) and moments (Mx, My, and Mz) measurements which were used to compare to the simulation results.

Table 2.3 Simulation test matrix for the first MTB tunnel entry.

# of Rotors	Tunnel Speed [ft/s]	MTB Rotor Config.	MTB Pitch [deg]
1	20, 40	Short	-10, -5, 0
2	20	Short	-10, -5, 0
4	20	Short	-10, -5, 0
6	20,40	Tall, Short	-10, -5, 0

2.2.2 Simulation test matrix of the 2nd MTB TE

The second MTB tunnel entry will focus on predicting the quadrotor configuration results. The quadrotor concept vehicle was part of the effort to study the trade-offs and performance of a variety of VTOL Urban Air Mobility (UAM) vehicles [Ref.15][Ref.16]. Figure 2.1 (a) and (d), shows the quadrotor reference model developed by the NASA Revolutionary Vertical Lift Technology (RVLT) Project. The quadrotor was designed to carry six occupants at a total weight of 1200 lb. This model has four rotors, and the height of the rear rotor is approximately 0.35*R higher than the front rotors, with each rotor tilted forward 3 deg in its neutral position.

In order to simulate the conceptual quadrotor design using the MTB, the conceptual quadrotor was scaled down by the rotor size, going from 18 ft to 24.5 inch diameter rotors. Using the rotor size as the scaling factor retains the same distance between the front and back rotors. The MTB is able to match the vertical, longitudinal, and lateral positions of the rotors (scaled conceptual quadrotor dimensions) to within +/- 0.4 inches.

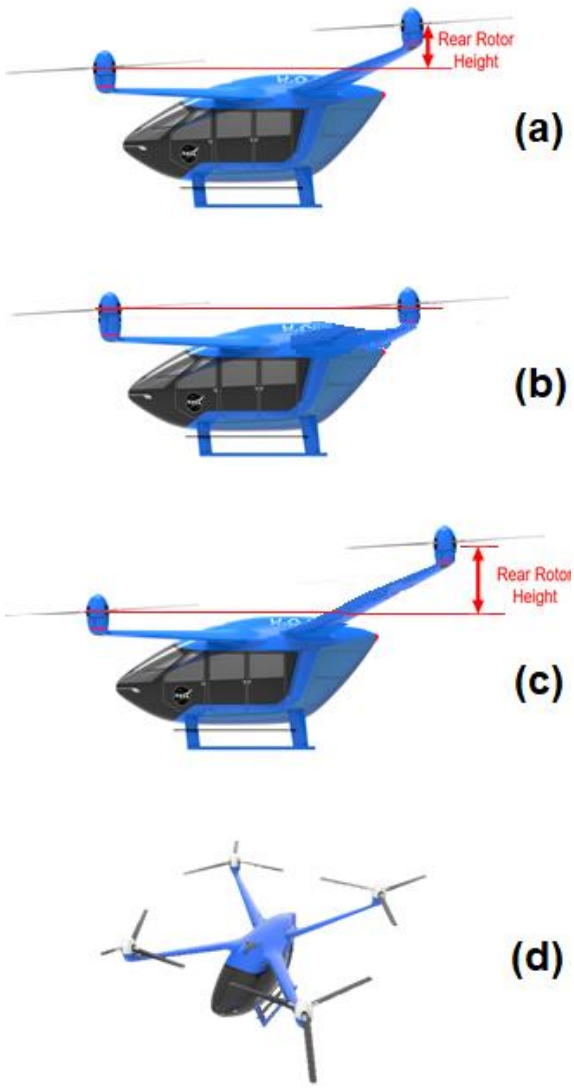

Figure 2.1 NASA UAM Quadrotor concept vehicle at, (a) original height, (b) zero rear rotor height (short), (c) maximum rear rotor height (tall), (d) isometric view of the quadrotor.

One of the main points of interest for the conceptual quadrotor design is the height difference between the front and the back rotors. The conceptual quadrotor has the front rotors lower than the back rotors to minimize the rotor wake interaction between the front and back rotors. In this paper, the quadrotor was simulated in CHARM and RotCFD in three different configurations: original conceptual quadrotor, short quadrotor, and tall quadrotor. The original conceptual quadrotor is the scaled down conceptual quadrotor, with its rotor positions within the possible MTB limits. The short quadrotor is the same as the original quadrotor, except the back rotors are at the same height as the front rotors, i.e. all rotors are in the same rotor disk plane. The tall quadrotor is the same as the original quadrotor, except the back rotors are in the highest position that the MTB can safely reach in the US Army 7-by 10-Foot wind tunnel. See Figure 2.1 for images of the different quad configurations.

As shown in the simulation test matrix in Table 2.4, each of the three quadrotor configurations were simulated for -10, -5 and 0 deg pitch for wind tunnel speeds of 0, 20, and 40 ft/s. A CAD model of the conceptual quadrotor was scaled down and used to run TwithB cases (only for the original height configuration in RotCFD). The TwithB cases were then compared to the TnoB cases to determine the effect of the body on the rotor performance. TnoB and FF cases were performed for both CHARM and RotCFD for all three rotor configurations.

Table 2.4 Simulation test matrix for the second MTB tunnel entry.

# of Rotors	Tunnel Speed [ft/s]	Quad Rotor Config.	Quad Pitch [deg]
4	0, 20, 40	Original Height	-10, -5, 0
4	0, 20, 40	Short	-10, -5, 0
4	0, 20, 40	Tall	-10, -5, 0

2.3 RotCFD Method

The RotCFD cases used the experimental values and tunnel conditions outlined in the previous section in order to match the experimental conditions as accurately as possible in the simulation domain. The physical simulation time was set to the time required for the freestream velocity to traverse the domain (in the x-direction) twice. The boundary was made larger than the actual wind tunnel test section (which is only 15ft long) in order to ensure that the flow had enough time and space to properly develop. In the present study the test section length was extended to 36.5 ft (11.13 m). For the present study, 20,000 timesteps were sufficient for converging the rotor performance.

The objective in generating the grid for the RotCFD simulations, was to find a balance between the accuracy of the results, computational budget, and time availability. Care was taken to ensure that the grid around the body of the MTB and the rotors remained the same throughout all cases. This was done to reduce the potential of additional inaccuracies and to increase the confidence in the comparisons between cases. For additional information on the grid generation for the RotCFD cases, see Reference 11.

The cases were run on the Pleiades supercomputer at NASA Ames Research Center. RotCFD can be run on standard workstations, but was run on Pleiades in order to complete several cases simultaneously in a short time period. Each case was run on a single Sandybridge+GPU node of the Pleiades computer. Using the node's NVIDIA Tesla K40 accelerator, RotUNS achieved performance on the order of 10-45 wall-clock seconds per timestep (about four days total per case on average). Since many of these nodes were available on the Pleiades computer, the cases were run in parallel and all cases were completed in approximately two weeks.

2.4 CHARM Method

The flight condition and rotor parameters have been defined using five CHARM input files. For each simulation case, the air density was adjusted to the recorded value at the time of wind tunnel testing to provide a similar condition to the wind tunnel test. The MTB rotor system was a fixed pitch rotor; therefore, the collective angle is fixed, and the KDE rotor was defined as a rigid, hingeless rotor in the rotor wake input file. The KDE rotor geometry changes from the root to the tip. Therefore, 24 aerodynamic sections are used to define the rotor geometry to increase simulation accuracy and more accurately model the blade's actual geometry. Due to the lack of information about the KDE rotor frequency modes, these settings were taken from a blade dynamics input file of a similar rotor (SUI) that had been validated in CHARM. In this study, the blade dynamics are solved in frequency space using the harmonic analysis solution, and all simulations used the lifting surface vortex lattice method [Ref.22], with 2D airfoil lookup tables to recover the lift curve and zero lift angle. Note that the quality of the 2D airfoil lookup tables is crucial for the accuracy of the prediction. The airfoil lookup tables must cover all the Mach numbers of any blade section that might occur during the CHARM calculation. CHARM is capable of calculating the Reynolds number correction from the lookup tables for each flight condition. The Mach numbers in CHARM should run from 0 to 1 to cover every possible flight condition; however, there was no airfoil table available for the KDE rotor at Mach number 1. Therefore, the highest Mach number in Table 2.2 was repeated to present the lookup table for the sonic Mach. A typical CHARM simulation for a 6 rotor case required less than 17 minutes.

3. SIMULATION RESULTS OF THE FIRST MTB TUNNEL ENTRY

The objective of the first MTB wind tunnel entry was to perform a systems checkout test and demonstrate all the capabilities of the MTB, i.e. testing with 1, 2, 4, and 6 rotors, tilting the rotors, pitching the whole model, moving the rotors in different positions/configurations, and testing at wind tunnel speeds of 0, 20, and 40 ft/s. The experimental thrust and torque values were taken from the recorded force and moment values from the six-axis load cells. The load cells were positioned underneath each rotor assembly, and tilt with the rotor (i.e. the rotor coordinate system always aligned with the load cell coordinate system along the z-axis). The experimental data was post-processed for load cell drift (see section 5 for more details) and was used to compare to the CHARM and RotCFD results.

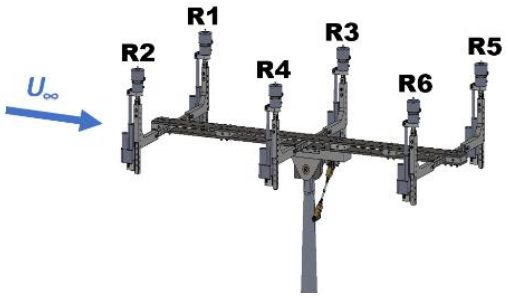

Figure 3.1 Rotor identification numbers.

The rotor numbers and wind direction are shown in Figure 3.1. The rotors are numbered beginning with the upstream rotors. Rotors 1, 4, and 5 are spinning counter-clockwise. Rotors 2, 3, and 6 are turning clockwise to cancel out the moments.

3.1 Isolated Rotor in Hover

The only experimental hover data currently available for the MTB is from Run 121, Point 5, in the 7-by 10 with the MTB at zero degree pitch angle and Rotor 2 operating at 2000 RPM. To simulate the isolated KDE rotor in RotCFD and CHARM, the RPM of a single rotor (no other rotors installed on the MTB) was varied between 500 and 6,000 RPM in hover without the presence of the MTB or wind tunnel walls. The single experimental data point was plotted against the values from the predicted RotCFD and CHARM isolated rotor cases. Figure 3.2 shows the correlation between the simulated results and the experimental data point for the Figure of Merit. The correlation between the C_P/σ and C_T/σ for RotCFD and CHARM are shown in Figure 3.3. It should be noted that the experimental data point was taken inside the tunnel whereas the

simulations were done in free field (FF) conditions (expanded domain boundary with no tunnel or MTB body in the simulation). The CHARM results show a higher FOM that is more aligned with the single experimental data point, and the RotCFD results show a lower FOM. The FOM computed from CHARM starts to decrease as rotor speed gets very high (over 4000 RPM), but RotCFD continues to increase and starts to plateau as the rotor reaches 6000 RPM. Future MTB testing will include more isolated rotor testing so that the rotor model can be further validated in hover.

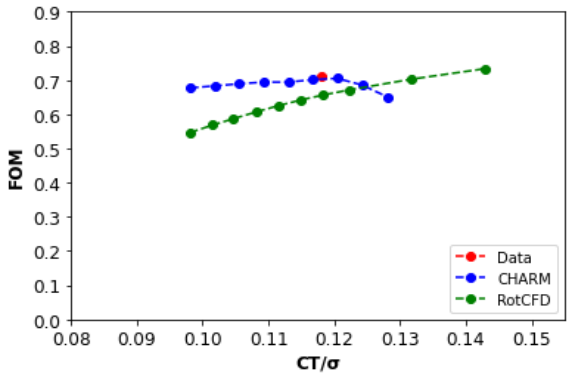

Figure 3.2 Single rotor in hover – Figure of Merit vs C_T/σ.

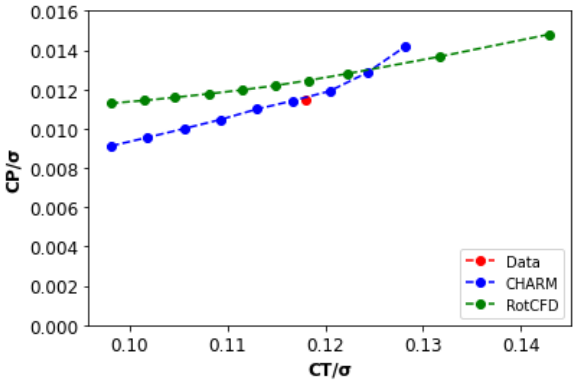

Figure 3.3 Single rotor in hover – C_P/σ vs C_T/σ.

3.2 Single Rotor in Forward Flight

The single rotor cases were run with rotor 2 (front port side) and were simulated for -10, -5, and 0 deg MTB pitch angle, at 20 ft/s and 40 ft/s tunnel RotCFD and CHARM results are compared to each other and to the experimental data. Since CHARM surface panel analysis requires more aerodynamic parts, such as a prop or a wing, the MTB chassis and rotor support hardware were not able to be modeled in CHARM. Therefore, only the TnoB and FF cases will be used to compare CHARM and RotCFD.

Looking at the RotCFD cases first, the effect of the body, as well as the tunnel, can be observed in Figures 3.4-3.7 for thrust and torque. There is little difference between the TwithB and TnoB cases both for thrust and for torque, although the thrust difference observed is greater for higher wind tunnel speeds. This suggests that for the single rotor cases, the body has a negligible effect on rotor performance. Both for thrust and torque, the FF cases have the largest difference from the experimental values at 0 deg pitch angle. This indicates that the tunnel has a more significant effect on the rotor performance at pitch angles closer to 0. Although the TwithB cases did show a slightly better correlation to the experimental data than the TnoB cases, the TnoB cases will be used to compare the CHARM and RotCFD values, in order to more fairly compare the two tools.

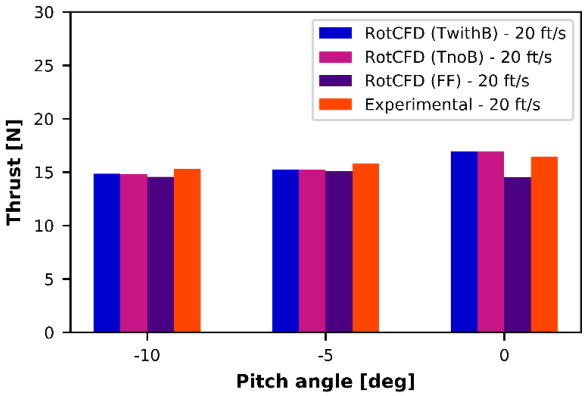

Figure 3.4 Single Rotor – CHARM – Thrust – 20ft/s.

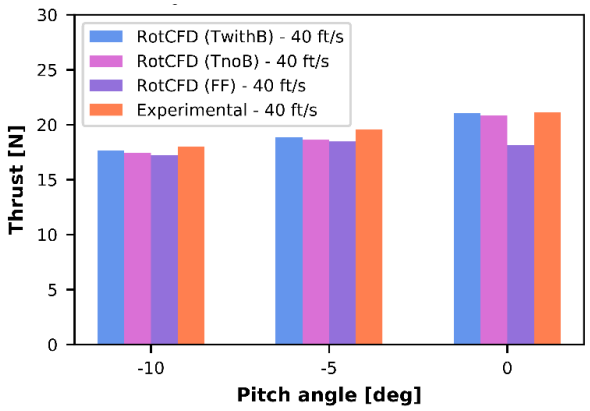

Figure 3.5 Single Rotor – RotCFD – Thrust – 40ft/s.

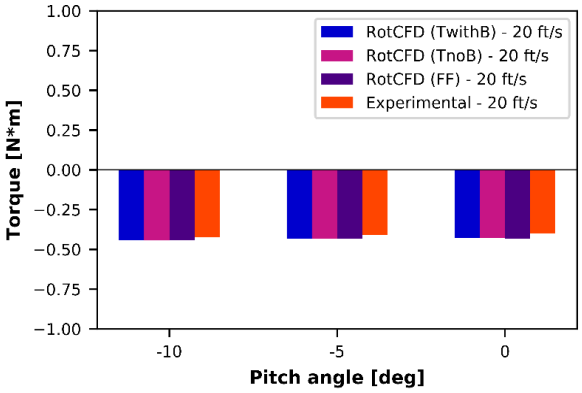

Figure 3.6 Single Rotor – RotCFD – Torque – 20ft/s.

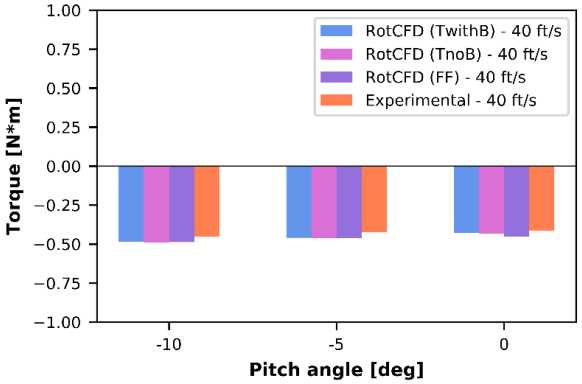

Figure 3.7 Single Rotor – RotCFD – Torque – 40ft/s.

Figures 3.8-3.11 show the CHARM results. The TnoB and FF cases are very similar and become more similar for the higher wind tunnel speed cases both for thrust and torque; see Figures 3.8-3.9 for thrust and 3.10-3.11 for torque. This trend is opposite to that observed in the previous RotCFD results. However, one similarity between the RotCFD and CHARM results is that the FF cases tended to predict lower thrust values than the TnoB cases, indicating that including the tunnel walls in the simulation causes an increase in thrust.

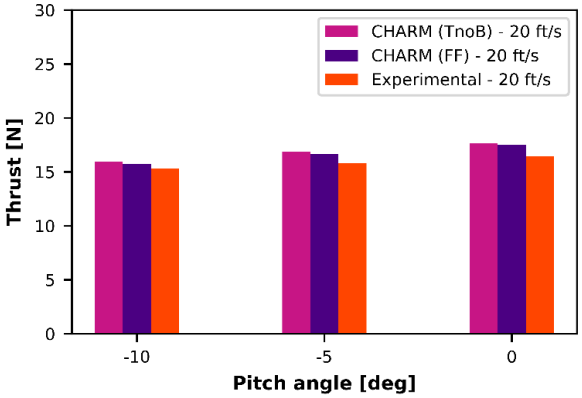

Figure 3.8 Single Rotor – CHARM – Thrust – 20ft/s.

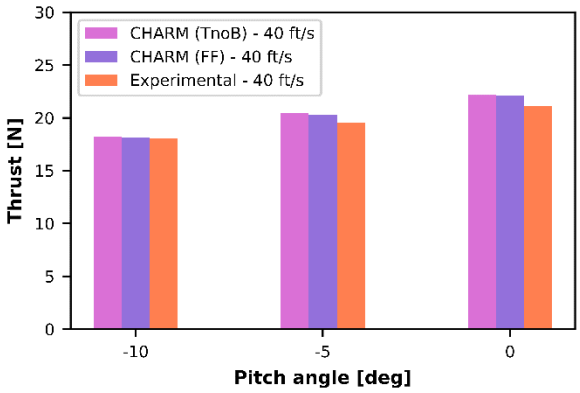

Figure 3.9 Single Rotor – CHARM – Thrust – 40ft/s.

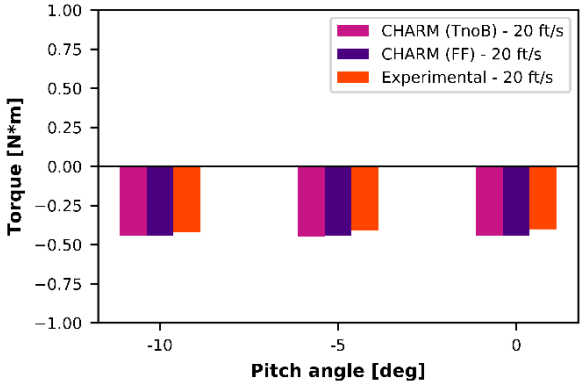

Figure 3.10 Single Rotor – CHARM – Torque – 20ft/s.

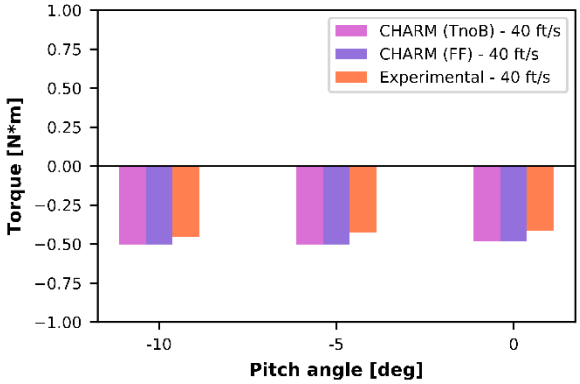

Figure 3.11 Single Rotor – CHARM – Torque – 40ft/s.

In order to more easily compare the RotCFD and CHARM values to each other and the experimental data, the discrepancies for each simulation result with respect to the experimental value were computed using the following equation:

$$\text{Discrepancy} = \left(1 - \frac{\text{Simulation}}{\text{Experimental}}\right) \text{x } 100\,\% \qquad (3.1)$$

Figures 3.12 and 3.13 show that for the single rotor cases, RotCFD tended to correlate better to the experimental data than CHARM. Additionally, the discrepancies both for RotCFD and CHARM tended to increase with tunnel speed. For most of the thrust values, RotCFD tended to under-predict, and CHARM tended to over-predict. For all of the torque values, both RotCFD and CHARM over-predicted.

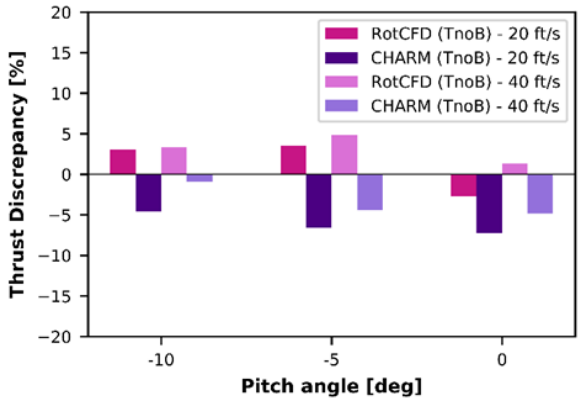

Figure 3.12 Single Rotor – CHARM vs RotCFD – Thrust.

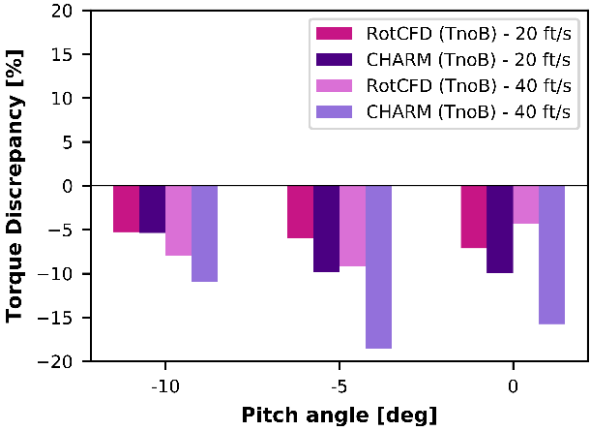

Figure 3.13 Single Rotor – CHARM vs RotCFD – Torque.

3.3 Four Rotors in Forward Flight

Rotors 1, 2, 3, and 4, were simulated for the four-rotor cases for -10, -5, and 0 deg MTB pitch angle, at 20 ft/s tunnel speed, in the short rotor configuration. For RotCFD, both TwithB and TnoB cases were run, to determine the effects of the body on the rotor performance. The TwithB and TnoB values were within 0.52% of each other for the four rotor cases, thus suggesting that the body has very little effect on the rotor performance for the four-rotor cases. However, the TnoB cases versus the FF cases were slightly different, particularly for the 0 deg pitch angle cases. The thrust values from the TnoB and FF cases differed from each other by a maximum 14.2% and on average 5.5% for RotCFD. This suggests that the tunnel has more of an effect on the rotor performance than the body. The CHARM thrust values between the TnoB and FF cases differed from each other by a maximum of 5.93% and on average 2.3%. Though the magnitude of the tunnel wall effects computed by RotCFD and CHARM are different, both codes infer that the tunnel walls should be included in the simulations.

Figures 3.14 and 3.15 show the discrepancies between the TnoB RotCFD and CHARM values to the experimental data for thrust and torque, respectively. Only the results for -10 deg and 0 deg pitch angle are shown, so the discrepancies for the individual rotors could be seen. There is no clear trend for the data. Overall, the RotCFD values show slightly better correlation to the experimental data.

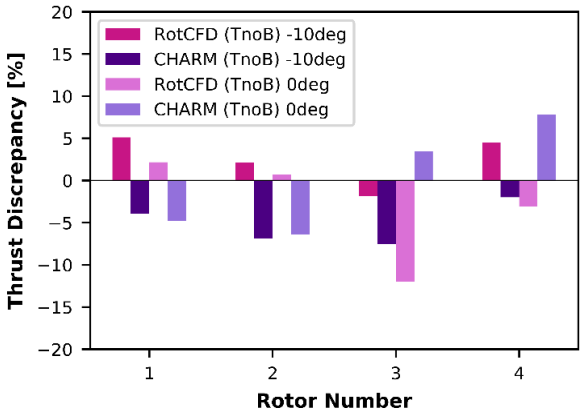

Figure 3.14 Four Rotors – CHARM vs RotCFD – Thrust.

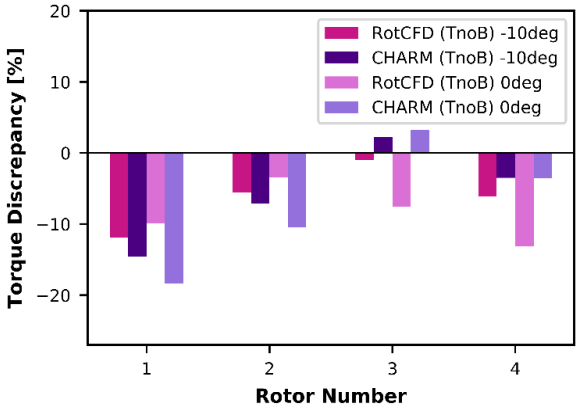

Figure 3.15 Four Rotors – CHARM vs RotCFD – Torque.

Table 3.1 shows the average discrepancies (averaged across the four rotors) for each case. The discrepancy

averages for RotCFD and CHARM are very similar. There is no clear trend for the thrust. The discrepancy averages for torque seem to increase as the pitch angle goes from -10 deg to 0 deg for both RotCFD and CHARM.

Table 3.1 Average rotor discrepancies for four-rotor cases at wind tunnel (TnoB) in forward flight.

		RotCFD	CHARM	Pitch [Deg]	V [ft/s]
Ave. Discrepancy	Thrust	3.41	5.09	-10	20
		6.40	4.62	-5	20
		4.48	5.62	0	20
	Torque	6.16	6.89	-10	20
		6.23	7.48	-5	20
		8.52	8.90	0	20

3.4 Six Rotors in Forward Flight

For the six-rotor cases, simulation studies were performed with the rotors in the MTB's tall rotor configuration and the short rotor configuration. The tall and short configurations refer to the vertical positioning of the rotors on the MTB structure in the tunnel. These cases were simulated at FF, TnoB, TwithB in RotCFD and FF, TnoB in CHARM in forward flight at speeds of 20 ft/s and 40 ft/s and at pitch angles of -10, -5, and 0 deg.

3.4.1 Six rotors in short configuration

The average discrepancy between the simulation results and the experimental data for thrust and torque values are shown in Table 3.2. The average discrepancy is the average of the absolute values of the individual rotor discrepancies for each case.

The TwithB and TnoB RotCFD values for thrust and torque were within 1.6% and 1.5% of each other, respectively, further showing that the body does not play a significant role on the rotor performance. Thus, continuing to use the TnoB cases instead of the TwithB cases would result in a fairly small error, assuming the TwithB cases to be more accurate. The average difference between the TnoB and FF RotCFD values for thrust and torque were 5.4% and 1.2%, respectively. The average difference between the TnoB and FF CHARM values for thrust and torque were 8.0% and 7.4% respectively. Both the RotCFD and CHARM results agree with the previous results that the tunnel plays a significant role in the rotor performance.

The RotCFD and CHARM discrepancies for thrust are lowest for the -10 deg pitch and 40 ft/s case, as shown in Figure 3.16. The RotCFD and CHARM discrepancies for thrust are higher for the 0 deg pitch and 40 ft/s case, Figure 3.17. Table 3.2 shows that CHARM had a better thrust prediction for these two TnoB cases (-10 deg and 0 deg pitch at 40ft/s). The reason for the increased discrepancy for the 0 deg results of both codes is most likely due to how each analysis simulates the rotor-wake interactions. The discrepancies for the 0 deg pitch and 40ft/s case are significantly higher on the downstream rotors as they are operating in the complex combined wakes of the front rotors. When the MTB is not pitched (at 0 deg) the wakes from the front rotors are convected downstream and increase wake interaction with rotors behind them (3 through 6). When the MTB is pitched forward (-10 deg), the wake from the front rotors travels below the following rotors, and therefore there is less wake interaction. If the simulation is not accurately modeling the wake interaction from the front rotors to the back, it could explain why the discrepancy is higher for the 0 deg pitch angle than the -10 deg pitch angle.

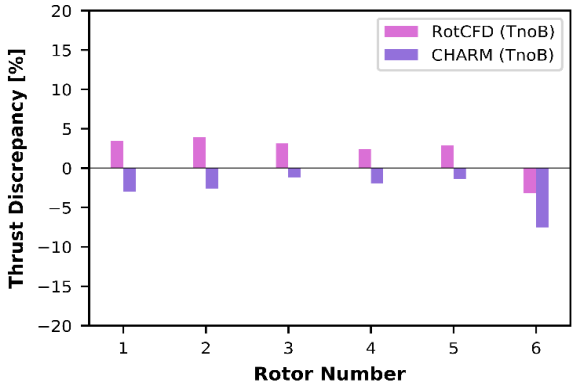

Figure 3.16 Six Rotors Short – Discrepancies – Thrust (-10 deg, 40 ft/s).

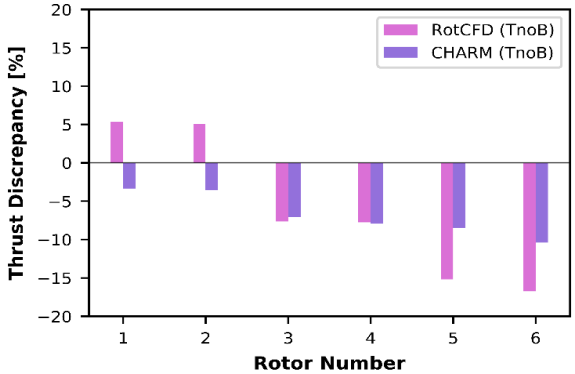

Figure 3.17 Six Rotors Short – Discrepancies – Thrust (0 deg, 40 ft/s)

These results can also be seen in Table 3.2, which shows the average discrepancy (averaged between the rotors) for all cases for thrust and torque. Overall, RotCFD, with the higher-fidelity wake simulation, provides better correlation with experimental values than does CHARM, which uses a free wake model. Results for the 20 ft/s cases can be observed in Table 3.2 but plots are not included for the conciseness of this paper.

Table 3.2 Average rotor discrepancies for six-rotor short cases in wind tunnel (TnoB) in forward flight.

		RotCFD	CHARM	Pitch [Deg]	V [ft/s]
Average Discrepancy	Thrust	4.84%	6.28%	-10	20
		3.02%	6.51%	-5	20
		5.82%	8.24%	0	20
		3.16%	2.96%	-10	40
		2.78%	7.24%	-5	40
		9.63%	6.81%	0	40
	Torque	4.74%	5.79%	-10	20
		4.63%	7.16%	-5	20
		7.55%	8.28%	0	20
		4.86%	7.15%	-10	40
		4.90%	11.99%	-5	40
		6.22%	11.85%	0	40

3.4.2 Six rotors in tall configuration

CHARM and RotCFD also simulated the six rotors in their tall configuration. For the conciseness of this paper, the cases for 20ft/s are not presented, but the results can be observed in Table 3.3. For the higher speed of 40 ft/s, the same trend from the previous section is observed (higher discrepancies for thrust on the back rotors), Figures 3.18 and 3.19.

For the -10 deg pitch and 40 ft/s case, the discrepancies for thrust for both RotCFD and CHARM are quite low. For the 0 deg pitch and 40 ft/s case, the discrepancies for the CHARM results are significantly higher for the back rotors than for the front rotors. The RotCFD results for the 0 deg pitch and 40 ft/s case tended to under-predict the front rotors and over-predict the back rotors. The over-prediction of the back rotors could be due to RotCFD not modeling the wake interaction from the front rotors as accurately (i.e. the wake from the front rotors would cause a reduced performance on the back rotors, thus decreasing the produced thrust). The discrepancies being higher on the back rotors for CHARM in the 0 deg pitch case also suggest that both simulations may not be as accurately modeling the rotor wake interaction on the back rotors. Table 3.3, shows the rotor-averaged discrepancy values for thrust and torque for the different cases.

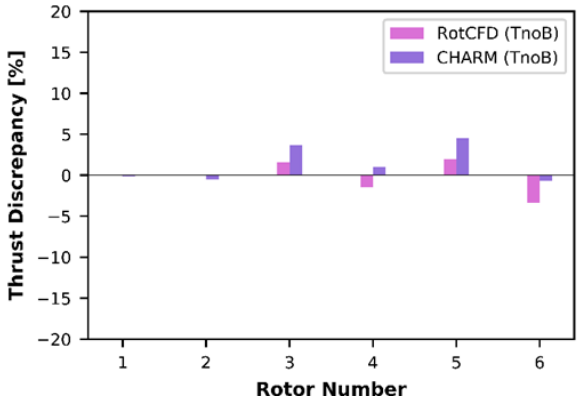

Figure 3.18 Six Rotors Tall – Discrepancies – Thrust (-10 deg, 40 ft/s).

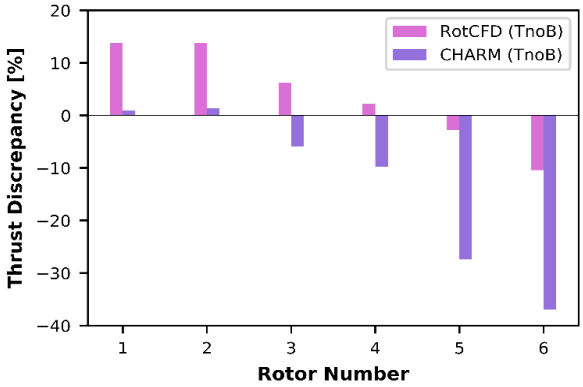

Figure 3.19 Six Rotors Tall – Discrepancies – Thrust (0 deg, 40 ft/s).

Table 3.3 Average rotor discrepancies for six-rotor tall cases in wind tunnel (TnoB) in forward flight.

		RotCFD	CHARM	Pitch [Deg]	V [ft/s]
Average Discrepancy	Thrust	1.52%	12.70%	-10	20
		1.65%	5.94%	-5	20
		7.04%	5.54%	0	20
		1.41%	1.76%	-10	40
		1.88%	2.20%	-5	40
		8.21%	13.73%	0	40
	Torque	4.15%	9.87%	-10	20
		4.68%	6.65%	-5	20
		6.42%	8.05%	0	20
		4.37%	4.71%	-10	40
		5.01%	5.89%	-5	40
		7.49%	4.41%	0	40

4. PRE-TEST SIMULATION PREDICTIONS OF THE SECOND MTB TUNNEL ENTRY

In the previous section, CHARM and MTB simulation results were compared to experimental data obtained from the MTB's first tunnel entry in 2019. The MTB is scheduled for a second tunnel entry in the US Army 7-by 10-Foot wind tunnel in 2022. In this section, some of the MTB configurations that will likely be tested in the 2022 test are simulated by CHARM and RotCFD to predict performance trends. These pretest predictions will provide information on which configurations might yield more interesting results (e.g. better or worse rotor performance). Additionally, these results can help determine if a fuselage should be included for testing (if the body has a significant effect on the rotor performance), and which configurations might result in significant tunnel wall effects on performance.

The objective of the second MTB wind tunnel entry is to acquire data for existing and conceptual multirotor configurations that might be emerging in the UAM market. Similar to the results from the first MTB test, these data will serve to validate analysis tools and enable further understanding of the performance of these multirotor configurations. Also, the test results will inform conceptual design trade studies evaluating rotor positioning on a multirotor configuration.

The test matrix for the second MTB wind tunnel entry will focus primarily on several quadrotor configurations that will serve as surrogates to the RVLT quadrotor concept vehicle. Some of the conceptual quadrotor designs include fixed-pitch hingeless, collective-only hingeless, and collective controlled articulated. This study assumes the fixed-pitch hingeless design. The initial analysis on this vehicle has predicted that the quadrotor will have good performance in hover and forward flight. Due to these qualities, the quadrotor configuration is a great candidate for testing in the MTB second tunnel entry. The RVLT quadrotor [Ref.15][Ref.19] was optimized to decrease the power usage in forward flight by elevating the rotors in the back.

As outlined in section 2.2.2, CHARM and RotCFD simulated scaled versions of: the original conceptual quadrotor; a short quadrotor (rotors all the same height); and a tall quadrotor (back rotors in the tallest MTB configuration). Results were obtained for pitch angles of -10, -5, and 0 deg alpha, and for wind tunnel speeds of 0, 20, and 40 ft/s. The rotor speed of each rotor was fixed at 2000 RPM and the system of 4 rotors was not trimmed. This paper presents the pre-test predictions for wind tunnel speeds of 20 and 40 ft/s.

4.1 Original Quad

The dimensions of the original quad are about 2.7R longitudinally between the front and back rotors, 2.7R laterally between the port and starboard rotors, and 0.35R vertically between the front and back rotors. The rotors are all tilted forward -3 deg (nose down) in the neutral position. Note that for -10 and -5 deg pitch angle, the rotors are tilted -10 and -5 deg with respect to the x-axis, and for the 0 deg pitch angle, the rotors are tilted -3 deg with respect to the x-axis (neutral position). RotCFD simulated the scaled version of the original quad for TwithB, TnoB, and FF, for -10, -5, and 0 deg pitch angle, for 20 and 40 ft/s, and CHARM simulated the same for the TnoB and FF cases.

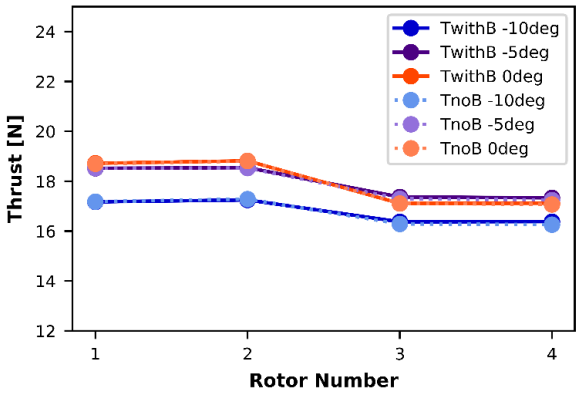

Figure 4.1 Original Quad – RotCFD – Thrust (40 ft/s).

For all angles and speeds, the maximum difference between the thrust and torque results for the TwithB and TnoB case were 0.96% and 0.38% respectively, implying that the quadrotor fuselage does not significantly affect the rotor performance. This could mean that a fuselage might not be necessary for the MTB wind tunnel entry 2. Figure 4.1 shows the TnoB cases overlapping with the TwithB cases for the different pitch angles for 40 ft/s, which indicates very little wake interaction between the fuselage and rotors.

Next, the influence of the tunnel is observed by looking at the difference between the TnoB cases and the FF cases for CHARM and RotCFD. The average difference between the TnoB and FF cases for the CHARM results for thrust and torque were 2.6% and 1.4% respectively. The average difference between the TnoB and FF cases for the RotCFD results for thrust and torque were 1.7% and 0.6% respectively. These average differences are slightly smaller but still similar to those of the 4-rotor simulations from the first tunnel

entry (5.5% for RotCFD and 2.3% for CHARM for thrust). These results indicate that the tunnel does have an effect on the rotor performance, but that it is less significant than in the previous 4-rotor cases examined from the first tunnel entry. Compared to the 4-rotor configuration, the Original Quad is more centered in the tunnel and the rotors are further away from the tunnel walls, reducing the influence of the tunnel walls. Figures 4.3 – 4.6 show the CHARM and RotCFD results for the TnoB and FF cases. For both CHARM and RotCFD, the thrust values are generally less for the FF cases than for the TnoB cases.

Figure 4.2 Flow visualization (showing U-velocity in m/s) of RotCFD simulation for original quad case, 20 ft/s tunnel speed, 0 deg pitch angle, with the quadrotor fuselage in the tunnel.

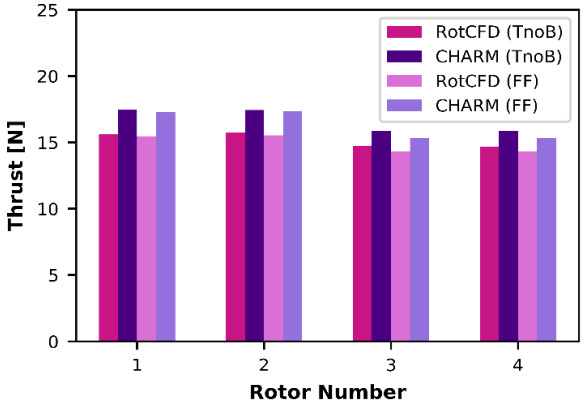

Figure 4.3 Original Quad –RotCFD and CHARM – TnoB vs FF – Thrust (-10 deg and 20 ft/s).

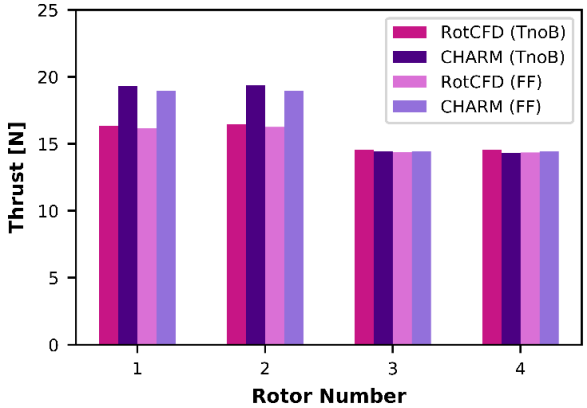

Figure 4.4 Original Quad –RotCFD and CHARM – TnoB vs FF – Thrust (0 deg and 20 ft/s).

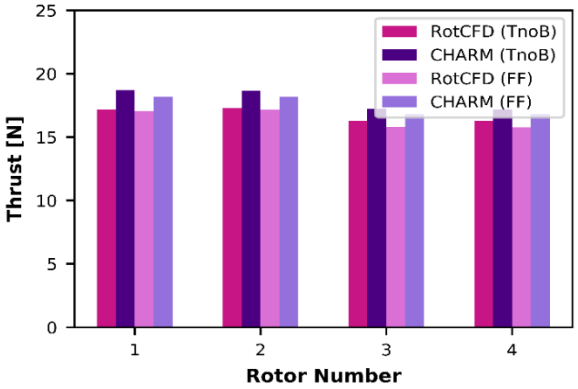

Figure 4.5 Original Quad –RotCFD and CHARM – TnoB vs FF – Thrust (-10 deg and 40 ft/s).

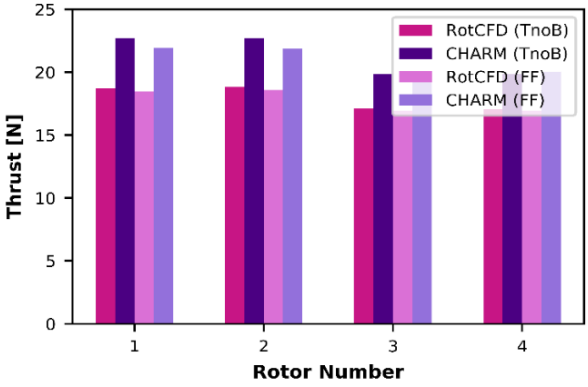

Figure 4.6 Original Quad –RotCFD and CHARM – TnoB vs FF – Thrust (0 deg and 40 ft/s).

The thrust results for RotCFD and CHARM for 20 and 40 ft/s at the different pitch angles are shown in Figures 4.7 and 4.8. CHARM tended to predict higher thrust values than RotCFD, but they both showed a similar trend for the pitch angles. A pitch angle of 0 deg had higher thrust than pitch angle of -10 deg, for all rotors. Additionally, both RotCFD and CHARM showed that rotors 1 and 2 had higher thrust values than the back rotors, 3 and 4. For both speeds, although more pronounced at 20 ft/s, the thrust decrease of the back rotors compared to the front rotors was greater for 0 deg pitch angle than for -10 deg pitch angle. This can be observed numerically in Figures 4.7 and 4.8, and the wake interaction of the front rotors with the back rotors can visually be seen in Figures 4.2 and 4.9. At 0 deg pitch angle, the front rotor wake interaction with the rear rotors increases, which causes a decrease in thrust generated by the rear rotors and thus decreasing rotor performance. Since the torque prediction results were all very similar for all cases, the plots were not presented in this paper; however, the average total values are presented in Tables 5.2 and 5.3.

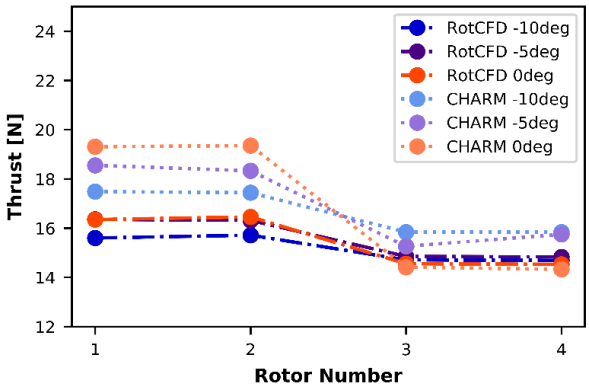

Figure 4.7 OG Quad –RotCFD and CHARM – Thrust (20 ft/s).

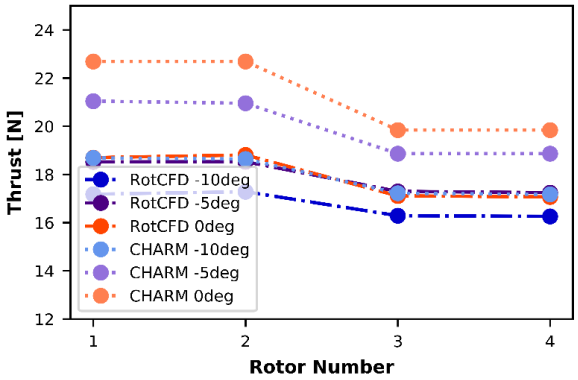

Figure 4.7 OG Quad –RotCFD and CHARM – Thrust (40 ft/s).

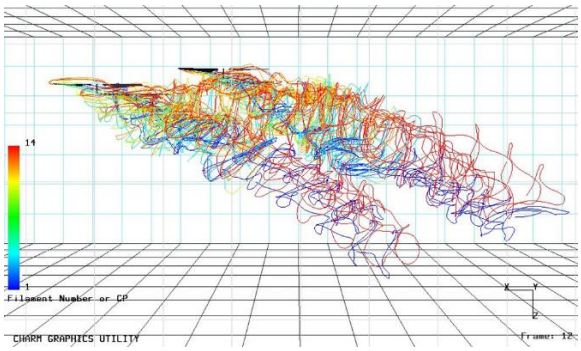

Figure 4.9 Flow visualization for the original quad at 20 ft/s tunnel speed, 0 deg pitch angle in the tunnel, was presented by inputting the CHARM solution into Vortex-X software.

4.2 Short Quad

The rotor positions for the short quad are the same as the original conceptual quad, except the back rotors are positioned at the same height as the front rotors at 0 deg pitch angle. The short quad configuration was simulated at -10, -5, and 0 deg pitch angle for forward flight speeds of 20 and 40 ft/s. Since in the previous section the fuselage was determined to have a very small effect on the rotor performance, the quadrotor fuselage is not simulated for the short and tall quad configurations.

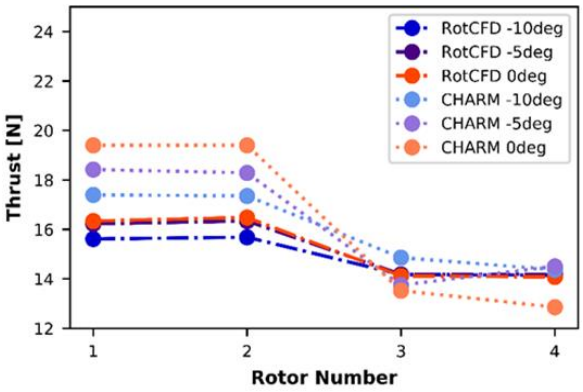

Figure 4.10 Short Quad –RotCFD and CHARM – Thrust (20 ft/s).

The RotCFD and CHARM results for thrust for 20 ft/s are shown in Figure 4.10. Comparing Figure 4.10 to the original quad results (Figure 4.7), the thrust for the front rotors (1 and 2) are about the same, but the thrust on the back rotors (3 and 4) has decreased significantly across all pitch angles, but more so for 0 deg pitch angle. Similar to the data from the first MTB test, the trends in Figure 4.10 are expected since the back rotors operate in the wakes of the front rotors, resulting in decreased rotor performance. A height difference between the front and back rotors clearly increases overall performance of the quadrotor.

4.3 Tall Quad

The rotor positions for the tall quad are the same as the original conceptual quad, except the back rotors assume the maximum height that the MTB will allow in the 7-by 10-Foot wind tunnel. The tall quad configuration was simulated for -10, -5, and 0 deg pitch angle as well as for forward flight at speed of 20 and 40 ft/s.

The RotCFD and CHARM results for the thrust for 20 ft/s are shown in Figure 4.11. Comparing again to the original quad in Figure 4.7, the thrust for the front rotors is about the same. However, here the thrust on the back rotors is higher for all cases. Similar to the original quad and short configuration, the biggest decrease in thrust going from the front to the back rotors occurs at 0 deg pitch angle. Increasing the vertical distance between the front and rear rotors will improve the rear rotors' performance. As a reminder, the rotors are not trimmed in the simulations. Although increasing the height between the front and back rotors

may lead to an increased thrust capability, the configuration may not be practical from a vehicle design or controls perspective.

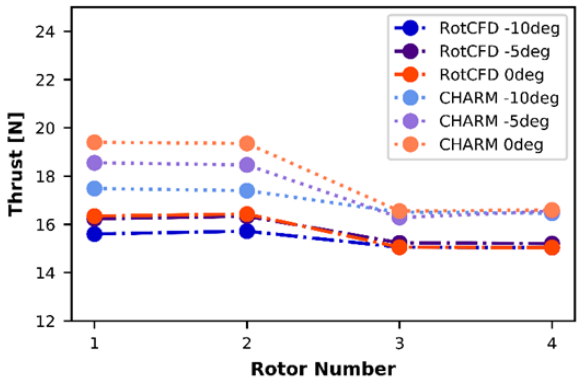

Figure 4.11 Tall Quad –RotCFD and CHARM – Thrust (20 ft/s).

5. POTENTIAL SOURCES OF ERROR

As with all experimental testing and simulations, there are potential sources of error. The simulation results indicate a wall effect; therefore, testing the MTB in a larger wind tunnel with the same size rotor could improve data measurements. The geometric dimensions of only one KDE rotor were used to create the airfoil tables for this study. All six KDE rotors could be laser scanned to more accurately measure the individual rotor geometries. Also, refining the airfoil tables could improve the correlation between simulations and experimental data, especially for CHARM, which is more sensitive to Reynolds number correction (note that RotCFD does not implement a Reynolds number correction). However, there will likely always be some error for both CHARM and RotCFD since they are using 2D airfoils to model complex 3D flow. The gridding in RotCFD is too coarse to capture higher order effects. Additionally, the tip-loss factor could be different for these smaller rotors compared to larger more conventional rotors. The tip loss factor used in the RotCFD simulations was 95%. The rotor model (particularly at the tip of the rotor) could significantly affect the results. For CHARM, a better blade dynamics input file needs to be created with information such as frequency modes for the KDE rotor. The exact measured RPM was used in the RotCFD simulations, but the CHARM simulations used 2000 RPM. However, this is not likely to contribute to a significant error since the RPM values were extremely close to 2000 RPM.

There are some potential sources of error with regards to the experimental data, which are being corrected for the MTB's second wind tunnel entry. A slight drift was observed in the experimental data, likely due to thermal changes during the runs and/or the load cell amplifiers. The data were corrected for this drift, which seemed to be monotonic over the course of a run. The amount of drift was assumed to change linearly from the initial static point (taken at the beginning of each run) to the final static point (taken at the end of each run). The interpolated drift was then subtracted from the data, and this corrected data is presented as the experimental data in this paper. For future MTB testing, thermocouples will be installed on the upper and lower surfaces of the load cells in order to more accurately monitor the temperature (and the drift) and the load cell amplifiers will be replaced with a less drift-prone version. A post-test check loading sequence of the load cells was performed as well, but the changes in the results from the check loads were insignificant on the thrust and torque measurements compared to that from the drift.

6. CONCLUSION

RotCFD and CHARM analyses were used to simulate several different multirotor configurations. RotCFD is a mid-fidelity CFD analysis while CHARM is a comprehensive rotorcraft analysis. Both use approximations in modeling the rotor aerodynamics. The characteristics of RotCFD, CHARM, and both simulation tools are listed below.

RotCFD:

- Runs slower than CHARM
- Can model fuselages and other non-rotating bodies easily
- Can manually adjust the grid
- Rotor solution and flow field computed via ADM, BEM, and URANS
- No Reynolds number correction
- User friendly, intuitive GUI

CHARM:

- Runs faster and uses less CPU and memory than RotCFD
- Difficult to model fuselages and other non-rotating bodies
- Uses the Hierarchical Fast Vortex approach to model wakes and determine aerodynamic interactions
- Sensitive to Reynolds number correction
- Uses the potential flow/panel method as an inviscid calculation

Both:

- Use 2D airfoils to model complex 3D flow, so cannot capture higher order effects
- Significantly faster and cheaper than higher-fidelity CFD
- Can mimic testing conditions (tunnel walls, airflow parameters, and rotor characteristics)

The simulation results were compared to experimental data from the 2019 MTB wind tunnel test. The analyses were also used to obtain pretest predictions for a second MTB test scheduled for 2022. RotCFD and CHARM have their advantages and disadvantages in simulating multirotor configurations. CHARM runs significantly faster than RotCFD but is limited in terms of modeling non-rotating bodies such as the MTB structure. However, the RotCFD results showed that in most cases, the body did not have a significant effect on the thrust or torque values (TwithB and TnoB results were within 1.6%). Increasing the number of rotors did increase the difference between the TwithB and TnoB cases, indicating that the body had a stronger effect on the rotor performance for an increased number of rotors. So, depending on the desired accuracy of the simulation and the number of rotors being used, the body may not be needed.

In this study, CHARM over predicted the power resulting from sensitivity to Reynolds number correction for values lower than 100,000. CHARM has been validated for predicting the thrust and power accurately for a single rotor. The torque prediction for the single KDE rotor was higher than expected, indicating the need for an improved 2D airfoil table.

Table 5.1 Average discrepancies for all MTB 1st wind tunnel entry simulations (TnoB) in forward flight.

	Ave. Thrust Discrepancy %		Ave. Torque Discrepancy %	
	RotCFD	CHARM	RotCFD	CHARM
One-Rotor	3.13	4.76	6.65	11.74
Two-Rotor	3.05	7.73	7.67	11.79
Four-Rotor	4.76	5.11	6.97	7.76
Six-Rotor(short)	4.88	6.34	5.48	8.71
Six-Rotor(tall)	3.62	6.98	5.35	6.60

Table 5.1 shows the average simulation discrepancies when compared to the data from the 2019 MTB test. The discrepancy values between RotCFD and CHARM are similar. There is no clear indication that increasing the number of rotors increases the discrepancy between the simulation and the experimental values. This implies that the simulation tools can reasonably model the interactional aerodynamics between the rotors and the tunnel. Note that these discrepancies are for the TnoB (in the tunnel without the body) cases.

The values in Table 5.1 were calculated by adding the thrust and torque values for the number of rotors for each case, and then averaging the values to give the average total thrust and torque discrepancies. For Table 5.2 and 5.3 the same was done, but the results were also averaged across the different pitch angles (-10, -5, and 0 deg) for tunnel speeds of 20 ft/s and 40 ft/s, respectively.

The pre-test predictions for the MTB second tunnel entry are shown in Tables 5.2 and 5.3. As mentioned previously, the torque values were about the same for all cases (original, short, tall, different pitch angles, and different speeds). Looking at the discrepancy values in Table 5.1 for the four-rotor configurations, it can be assumed that the values in Table 5.2 are accurate within about 4-8%. These results indicate that both RotCFD and CHARM are good tools for quickly predicting multirotor performance.

Table 5.2 Average thrust and torque predictions for the quadrotor configurations in wind tunnel (TnoB) for 20ft/s for all pitch angles.

	Average Thrust [N]		Average torque [N*m]	
	RotCFD	CHARM	RotCFD	CHARM
Original	61.64	67.29	1.80	1.83
Short	60.51	64.69	1.81	1.80
Tall	62.41	69.85	1.79	1.85

Table 5.3 Average thrust and torque predictions for the quadrotor configurations in wind tunnel (TnoB) for 40ft/s for all pitch angles.

	Average Thrust [N]		Average torque [N*m]	
	RotCFD	CHARM	RotCFD	CHARM
Original	70.08	78.82	1.85	1.99
Short	68.66	75.22	1.86	1.98
Tall	70.87	80.05	1.83	1.99

7. FUTURE WORK

Additional experimental hover testing for an isolated rotor should be performed to help validate the rotor model. Further work on the rotor model should be performed: modifying the simulated rotor geometry, blade tips, and tip loss factors. OVERFLOW software,

or other CFD analysis, could be used to generate improved airfoil tables.

Improvements are currently being made to the MTB to improve the quality of the data measurements for future MTB testing.

The predictions for the MTB test in 2022 will be used to help determine the final test matrix. Additional RotCFD and CHARM studies may be performed on other potential testing multirotor configurations.

ACKNOWLEDGMENTS

The authors would like to thank the following people for their contributions to this project. Thank you to William Warmbrodt for his continued outstanding leadership. Thank you to Carl Russell, who is the PI for the MTB program and the Test Director, as well as an amazing mentor. Thank you to Gloria Yamauchi for her guidance, mentorship, and logistical help in running simulations. Thank you to Dan Wachspress who gave so very generously of his knowledge and time. Thank you to Witold Koning for his unparalleled subject matter expertise and support with RotCFD, and to Kristen Kallstrom for generating the airfoil tables. Thank you to Ethan Romander for his help with running RotCFD cases on Pleiades. Thank you to Larry Young for his invaluable insight in all things RotCFD. Thank you to William Polzin who was an invaluable resource at Sukra Helitek, Inc. Thank you to Larry Meyn who developed the .c81 cleaner script. Gina Willink, lead of the Ames Aeromechanics Mechanical Systems Team, helped throughout the design process, reviewed the design and analysis, and provided invaluable advice. The NASA Machine Shop Team, led by Robert Kornienko and Vincent Derilo, machined the parts of the MTB and provided guidance and helpful suggestions during the design process. Steve Nance along with the other members of the 7- by 10-Foot Wind Tunnel test crew were critical to the project's success.

REFERENCES

[1] Russell, C., Willink, G., Theodore, C., and Glasner, B., "Wind Tunnel and Hover Performance Test Results for Multicopter UAS Vehicles," NASA/TM-2018-219758, February 2018.

[2] Russell, C., and et al, "Multicopter UAS Performance Test 2," NASA/TM (not yet published).

[3] Cheng, G., Nunez, G., Russell, C., Avera, M., and Dorrerweich, J., "Wind Tunnel Test Results for an Overlapped Quadrotor Configured UAS," presented at the AHS International 74th Annual Forum and Technology Display, Phoenix, AZ, May 2018.

[4] Russell, C., and Conley, S.,"The Multirotor Test Bed – A New NASA Test Capability for Advanced VTOL Rotorcraft Configurations," presented at the VFS 76th Annual Forum and Technology Display, Virginia Beach, VA, October 2020.

[5] Conley, S., and Russell, C., "Mechanical Design of the Multirotor Test Bed," Vertical Flight Society Aeromechanics for Advanced Vertical Flight Technical Meeting, San Jose, CA, January 2020.

[6] Rajagopalan, R. G., Thistle, J. R., and Polzin, W. J., "The Potential of GPU Computing for Design in RotCFD," presented at the AHS Technical Meeting on Aeromechanics Design for Transformative Vertical Flight, San Francisco, California, January 2018.

[7] Rajagopalan, R. G., and et al., "RotCFD - A Tool for Aerodynamic Interference of Rotors: Validation and Capabilities," presented at the American Helicopter Society Future Vertical Lift Aircraft Design Conference, San Francisco, CA, January 2012.

[8] Novak, L. A., Guntupalli, K., and Rajagopalan, R. G., "RotCFD: Advancements in Rotorcraft Modeling and Simulation," presented at the The 4th Asian/Australian Rotorcraft Forum, IISc, India, November 2015.

[9] Koning, W. J. F. ,"Wind Tunnel Interference Effects on Tiltrotor Testing Using Computational Fluid Dynamics," NASA/CR—2016–219086, March 2016.

[10] Koning, W. J. F., "Using RotCFD to Predict Isolated XV-15 Rotor Performance," presented at the AHS Technical Meeting on Aeromechanics Design for Vertical Lift, San Francisco, CA, January 2016.

[11] Conley, S., Russell, C., Kallstrom, K., Koning, W., and Romander, E., "Comparing CFD Predictions of the Multirotor Test Bed with Experimental Results," presented at the VFS 76th Annual Forum and Technology Display, Virginia Beach, VA, October 2020.

[12] Quackenbush, T. R., and Bliss, D. B., "Free Wake Calculation of Rotor Flow Fields for Interactional Aerodynamics," presented at the AHS 44th Annual Forum, Washington DC, June 1988.

[13] Wachspress, D. A., Quackenbush, T. R., and Boschitsch, A. H., "First-Principles Free-Vortex Wake Analysis for Helicopters and Tiltrotors,"

presented at the AHS 59th Annual Forum, Phoenix, AZ, May 2003.

[14] Choi, J. Y., Summers, M., and Corrigan, J. J., "Validation of CHARM Wake Methodology for Compu-tation of Loads and Vibrations," presented at the AHS 65th Annual Forum, May 2009.

[15] Silva, C., and et al, "VTOL Urban Air Mobility Concept Vehicles for Technology Development," AIAA AVIATION, AIAA 2018-3847, Dallas, TX, 2018.

[16] Ventura, D., and et al., "Computational Study of NASA's Quadrotor Urban Air Taxi Concept," AIAA SciTech, AIAA 2020-0302, Orlando, FL, 2020.

[17] Shirazi, D., "Wake Simulation of the Multirotor Test Bed and Validation of CHARM Software," NASA/TM (not yet published).

[18] Drela, M., "FOIL: An Analysis and Design System for Low Reynolds Number Airfoils in presented at the Conference on Low Reynolds Number Airfoil Aerodynamics," University of Notre Dame, June 1989.

[19] Johnson, W., Silva, C., and Solis, E., "Concept Vehicles for VTOL Air Taxi Operations," AHS Specialists' Conference on Aeromechanics Design for Transformative Vertical Flight, San Francisco, CA, 2018.

[20] Shirazi, D., "Wake Simulation of the Multirotor Test Bed and Validation of CHARM Software," Master Thesis, Mechanical and Aerospace Engineering Dept., California Irvine Univ., Irvine, CA , ProQuest (not yet published).

[21] Russell, C., and Sekula, M. K., "Comprehensive Analysis Modeling of Small-Scale UAS Rotors," 2017.